



ELSEVIER

26 July 2001

Physics Letters B 513 (2001) 23–29

PHYSICS LETTERS B

www.elsevier.com/locate/npe

# A new upper limit for the tau-neutrino magnetic moment

DONUT Collaboration

R. Schwienhorst<sup>a</sup>, D. Ciampa<sup>a</sup>, C. Erickson<sup>a</sup>, M. Graham<sup>a</sup>, K. Heller<sup>a</sup>, R. Rusack<sup>a</sup>,  
J. Sielaff<sup>a</sup>, J. Trammell<sup>a</sup>, J. Wilcox<sup>a</sup>, K. Kodama<sup>b</sup>, N. Ushida<sup>b</sup>, C. Andreopoulos<sup>c</sup>,  
N. Saoulidou<sup>c</sup>, G. Tzanakos<sup>c</sup>, P. Yager<sup>d</sup>, B. Baller<sup>e</sup>, D. Boehnlein<sup>e</sup>, W. Freeman<sup>e</sup>,  
B. Lundberg<sup>e</sup>, J. Morfin<sup>e</sup>, R. Rameika<sup>e</sup>, J.C. Yun<sup>e</sup>, J.S. Song<sup>f</sup>, C.S. Yoon<sup>f</sup>,  
S.H. Chung<sup>f</sup>, P. Berghaus<sup>g</sup>, M. Kubantsev<sup>g</sup>, N.W. Reay<sup>g</sup>, R. Sidwell<sup>g</sup>, N. Stanton<sup>g</sup>,  
S. Yoshida<sup>g</sup>, S. Aoki<sup>h</sup>, T. Hara<sup>h</sup>, J.T. Rhee<sup>i</sup>, K. Hoshino<sup>j</sup>, H. Jiko<sup>j</sup>, M. Miyanishi<sup>j</sup>,  
M. Komatsu<sup>j</sup>, M. Nakamura<sup>j</sup>, T. Nakano<sup>j</sup>, K. Niwa<sup>j</sup>, N. Nonaka<sup>j</sup>, K. Okada<sup>j</sup>,  
O. Sato<sup>j</sup>, T. Akdogan<sup>k</sup>, V. Paolone<sup>k</sup>, C. Rosenfeld<sup>k</sup>, A. Kulik<sup>k,l</sup>, T. Kafka<sup>m</sup>,  
W. Oliver<sup>m</sup>, T. Patzak<sup>m</sup>, J. Schneps<sup>m</sup>

<sup>a</sup> University of Minnesota MN, USA

<sup>b</sup> Aichi University of Education, Kariya, Japan

<sup>c</sup> University of Athens, Athens 15771, Greece

<sup>d</sup> University of California-Davis, Davis, CA 95616, USA

<sup>e</sup> Fermilab, Batavia, IL 60510, USA

<sup>f</sup> Gyeongsang National University, Jinju 660-701, South Korea

<sup>g</sup> Kansas State University, Manhattan, KS 66506, USA

<sup>h</sup> Kobe University, Kobe, Japan

<sup>i</sup> Kon-kuk University, South Korea

<sup>j</sup> Nagoya University, Nagoya 464-8602, Japan

<sup>k</sup> University of Pittsburgh, Pittsburgh, PA 15260, USA

<sup>l</sup> University of South Carolina, Columbia, SC 29208, USA

<sup>m</sup> Tufts University, Medford, MA 02155, USA

Received 26 February 2001; accepted 31 May 2001

Editor: K. Winter

## Abstract

Using a neutrino beam in which a  $\nu_\tau$  component was identified for the first time, the  $\nu_\tau$  magnetic moment was measured based on a search for an anomalous increase in the number of neutrino–electron interactions. One such event was observed when 2.3 were expected from background processes, giving an upper 90% confidence limit on  $\mu_{\nu_\tau}$  of  $3.9 \times 10^{-7} \mu_B$ . © 2001 Published by Elsevier Science B.V.

PACS: 14.60.Lm; 14.60.St; 13.40.Em

## 1. Introduction

Magnetic moment measurements are an important tool for probing the fundamental structure of matter. Currently, precision measurements of the electron and muon magnetic moments are being used to probe the structure of the vacuum to the highest precision. A non-zero magnetic moment for a neutrino would be a clear and unambiguous signal for physics beyond the Standard Model. We have used the data collected for the Fermilab experiment E872 (DONUT) to perform a search for anomalous electromagnetic interactions of the tau-neutrino that would be a signature for a magnetic moment. This Letter presents the first measurement of the  $\nu_\tau$  magnetic moment using a neutrino beam in which the  $\nu_\tau$ 's have been positively identified.

The direct limits on  $\nu_e$  and  $\nu_\mu$  magnetic moments are  $\mu_{\nu_e} < 1.8 \times 10^{-10} \mu_B$  [1] and  $\mu_{\nu_\mu} < 7.4 \times 10^{-10} \mu_B$  [2] and efforts are currently being made to extend these limits by another order of magnitude [3,4]. In the CERN experiment WA66 [5], a limit of  $\mu_{\nu_\tau} < 5.4 \times 10^{-7} \mu_B$  was based on a calculated flux of  $\nu_\tau$ 's in the neutrino beam [6]. Direct limits have also been set in electron–positron collider experiments through detailed studies of the process  $e^+e^- \rightarrow \nu\bar{\nu}\gamma$  [7–9]. Elsewhere, indirect limits for neutrino magnetic moments were derived from the duration of supernova explosion SN1987A, giving a limit of  $10^{-11} \mu_B$  for all neutrino flavors under the assumption that they are equally produced.

The growing evidence for neutrino oscillations implies that neutrinos are massive and that the weak eigenstates  $\nu_e$ ,  $\nu_\mu$  and  $\nu_\tau$  are mixtures of the mass eigenstates  $\nu_1$ ,  $\nu_2$  and  $\nu_3$  [10,11]. Consequently, the electromagnetic properties of neutrinos should be associated with the mass eigenstates rather than the weak eigenstates. Since the parameters of the mixing matrix are as yet undetermined, and there remains the possibility that neutrino mixing is further complicated by an additional sterile neutrino [12], the composition of any neutrino beam in terms of the mass eigenstates can at this stage not be determined. Until the oscillation scenario is fully understood, the electromagnetic properties should therefore be characterized by the initial neutrino flavor. This description is independent of neutrino energy and distance from the source and al-

lows for an extraction of the mass eigenstate magnetic moments once all of the mixing parameters are known [13].

It has been argued that  $\nu_\mu$ – $\nu_\tau$  mixing together with the current limit for  $\nu_\mu$  would give a limit of  $\mu_{\nu_\tau} < 1.9 \times 10^{-9} \mu_B$  [14]. This derived limit depends on the interpretation of oscillation experiments and does not use the convention of specifying the magnetic moment by the initial flavor state, which is adopted for our result.

In DONUT, the tau-neutrino magnetic moment would be measured as an anomalous increase in the elastic neutrino cross-section above the value predicted by the Standard Model. Tau neutrinos interact with electrons through  $Z^0$  exchange in the Standard Model, and a magnetic moment  $\mu_{\nu_\tau}$  adds an extra component due to photon exchange. The cross-section for a neutrino interacting via its magnetic moment with an electron is given in the high-energy limit by

$$\frac{d\sigma_\mu}{dT_e} = \frac{\mu_\nu^2}{\mu_B^2} \frac{\pi\alpha^2}{m_e^2} \left( \frac{1}{T_e} - \frac{1}{E_\nu} \right), \quad (1.1)$$

where  $T_e$  is the energy of the scattered electron in the laboratory frame [15]. The distribution of  $T_e$  for our  $\nu_\tau$  energy spectrum is shown in Fig. 1.

The total magnetic moment scattering cross-section is obtained by integrating over  $T_e$ , where the unphysical divergence at zero is avoided by introducing a low-

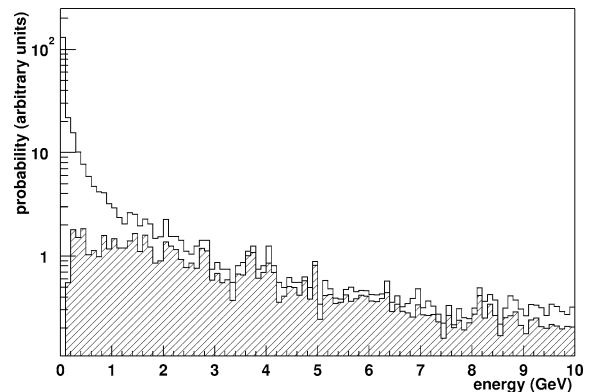


Fig. 1. Kinetic energy distribution for the electron produced in  $\nu_\tau$  magnetic moment interactions. The solid line shows the electron energy for Monte Carlo generated magnetic moment interactions (Eq. (1.1) folded with our  $\nu_\tau$  energy spectrum), while the shaded area shows the electron energy after all of the selection cuts.

energy cutoff  $T_e^{\min}$ . Since the neutrino undergoes a spin-flip when a photon is exchanged, there is no interference with the Standard Model process, and the total neutrino–electron scattering cross-section is just given by the sum of the two contributions.

Kinematic constraints [16] limit the angle between the incoming neutrino and the scattered electron in the laboratory frame to be

$$\theta_{\nu-e}^2 < \frac{2m_e}{E_e}, \quad (1.2)$$

and for electron energies in excess of about 1 GeV,  $\theta_{\nu-e}$  is less than 30 mrad. This angular constraint can be used as a clear signal to select neutrino–electron scattering events from the background of  $\nu_e$ -nucleon charged-current events in which the electron is produced at a much larger angle.

## 2. The apparatus

The DONUT experiment took data in 1997 and  $\nu_\tau$ -N charged-current interactions were observed in nuclear emulsion [17]. The apparatus is described in detail elsewhere [18]; only the components central to this analysis will be discussed here.

The experiment consisted of three essential parts, shown in Fig. 2: a  $\nu_\tau$  enriched neutrino beam, a neutrino target, and a spectrometer with electron and

muon identification. A “prompt” neutrino beam was produced by a beam of 800 GeV protons incident on a tungsten target. The target length and material were chosen so that most of the long-lived secondary particles would interact in the target before decaying, while the short-lived particles would decay before interacting. Hence the main contribution to the high-energy neutrino flux came from the decay of  $D$ -mesons. The primary source of  $\nu_\tau$  was the leptonic decay of a  $D_s$  into a  $\tau$  and  $\bar{\nu}_\tau$ , and the subsequent decay of the  $\tau$  to a  $\nu_\tau$ . It is estimated that in the sample of events located in the emulsion, the neutrino interactions would be 47%  $\nu_\mu$  charged-current events, 27%  $\nu_e$  charged-current events, 5%  $\nu_\tau$  charged-current events, and 21% neutral-current events. This composition was confirmed by our measurements of charged-current interactions [17].

Particles other than neutrinos originating in primary proton interactions, mostly muons, were absorbed or swept away from the neutrino target region using magnets together with concrete, iron, and lead shielding. Any remaining charged particles from the proton beam dump that passed through the neutrino target region were identified by a scintillation counter veto wall.

The neutrino target region, shown in Fig. 3, consisted of four emulsion modules that were interleaved with 44 planes of 0.5 mm diameter scintillating fibers. This scintillating fiber tracker (SFT) was used to reconstruct charged particle tracks from the neutrino

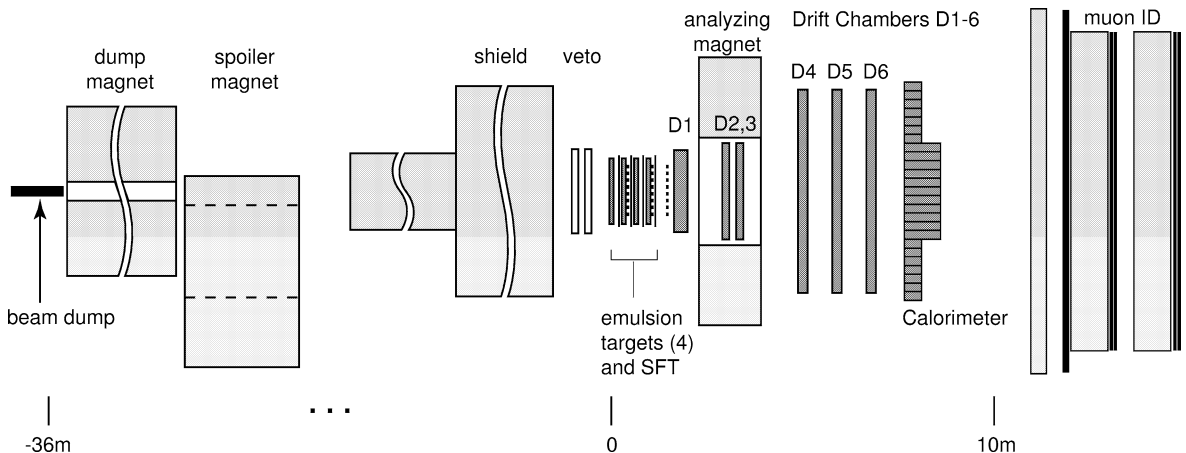


Fig. 2. Experimental beam and spectrometer. At the left, 800 GeV protons were incident on the beam dump, which was 36 m from the first emulsion module. Muon identification was done by range in the system on the right. The vertical scale is identical to the horizontal scale.

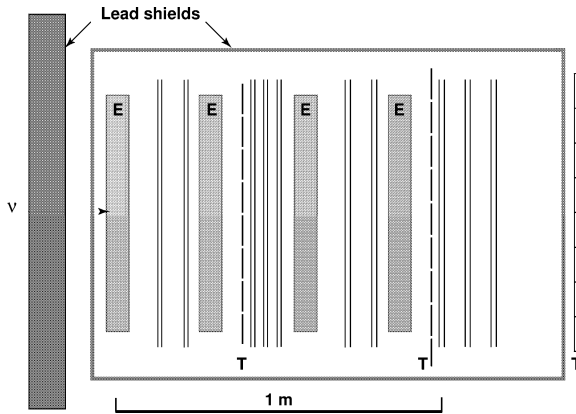


Fig. 3. Closeup view of the neutrino target region from Fig. 2. The emulsion modules are denoted by an “E”, the trigger planes by a “T”. Only scintillating fiber planes in one orientation are shown, they are represented by thin vertical lines. Also shown is the upstream lead wall and the target shielding box. The vertical scale is identical to the horizontal scale.

interaction vertex. The entire target region was surrounded by lead shielding, 20 mm thick on the upstream side and 6 mm thick on the other sides. Since the veto counters were upstream of this lead shield, neutrino interactions in the shield were allowed and the wall was considered part of the neutrino target.

The other components of the spectrometer were used for lepton identification and measurement of the event energy. Momenta of charge particles were measured through a combination of drift chambers and a wide-aperture magnet. A lead-glass calorimeter was used to measure the electromagnetic energy produced by a neutrino interaction and to identify electrons and minimum-ionizing particles. Muons were identified with an array of proportional tubes between three walls of iron.

The spectrometer readout was triggered by a signal pattern consistent with more than one charged track in the scintillation counter hodoscopes placed in the emulsion region, and no signal from the upstream veto wall.

### 3. Event selection

The final state of the neutrino–electron scattering process consists of a neutrino that leaves the apparatus

undetected and a single electron that travels at a small angle with respect to the incident neutrino direction. Each emulsion module presents between two and three radiation lengths in the direction of the neutrino beam. Consequently, most electrons that originate within an emulsion module have initiated an electromagnetic shower measured by the SFT. By contrast, the SFT presents only very little material in the direction of the beam. Thus, it provides a sample of the shower at a specific depth. The search for magnetic moment interactions must therefore rely on identifying electromagnetic showers through this characteristic pattern of charged particle tracks.

In the six-month run of the experiment  $4.0 \times 10^6$  events were recorded for analysis and  $2.0 \times 10^5$  of these had two or more reconstructed tracks in the target region. From this sample, magnetic moment candidate events were selected in a series of selection cuts, each using more detailed detector information than the previous one.

A large fraction of the events in the sample was not produced by neutrino interactions but by high-momentum muons that interacted in the material surrounding the target and its support system. These interactions sent secondary particles from the outside into the target area. Events were therefore rejected if any of the following requirements were met: there was a reconstructed muon in the event; the reconstructed vertex was not in the fiducial volume; none of the reconstructed tracks had an angle of less than 100 mrad with respect to the incoming neutrino direction. The fiducial volume was given by the dimensions of the emulsion modules with the additional requirement that the vertex was no more than 0.24 m in the transverse direction from the center of a module.

The remaining non-neutrino events were removed in a visual scan that selected events with a reconstructed neutrino interaction vertex with no upstream high momentum tracks. A total of 68 events were selected in the data set compared to 41 expected from a Monte Carlo simulation. The excess in the data was caused by interactions of low-energy neutrons or photons in the most downstream emulsion module. These events were removed by requiring a signal of at least 2 GeV in the lead-glass calorimeter, but only if the interaction vertex was in the most downstream emulsion module. This cut reduced the number of events to 29 in the data and 32 in the Monte Carlo.

Since all of the remaining events were produced by neutrino scattering, the selection cuts focussed on rejecting  $\nu$ -N events, which could be identified by the hadronic activity in the event. Since each emulsion module corresponded to a thickness of about 0.3 nuclear interaction lengths, hadrons typically passed through a module without producing shower particles. Furthermore, low-momentum hadrons produced large pulseheight signals in the SFT due to greater ionization. Events with reconstructed tracks that had large fiber pulseheights or passed through an emulsion module without creating a particle shower were therefore rejected.

Hadrons could also be identified in the electromagnetic calorimeter because they produced only a small signal compared to electrons of the same momentum. Consequently, events with momentum-analyzed tracks were rejected if the ratio of the measured track momentum to the signal in the electromagnetic calorimeter was less than 0.5.

Once these tests were applied only 13 events remained. Monte Carlo simulations showed that hadronic showers had a wider profile and more tracks at large angles than electromagnetic showers. Events were therefore selected if there was an identified electron at an angle of less than 30 mrad and if there were no reconstructed tracks with angles in excess of 500 mrad. This left one event, shown in Fig. 4, an interaction in the most downstream emulsion module.

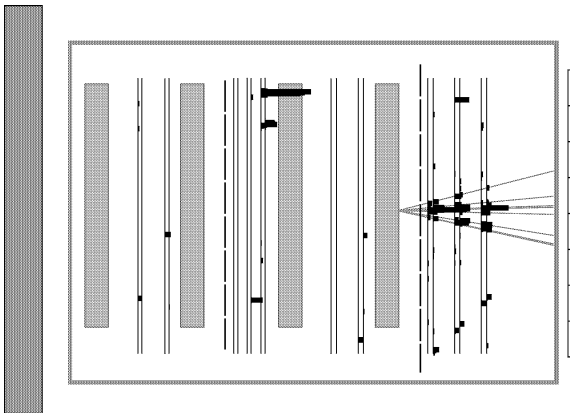


Fig. 4. Target region view of the selected magnetic moment candidate event. Shown are the hits in the scintillating fibers and the reconstructed tracks associated with the neutrino interaction.

#### 4. Data analysis

Magnetic moment interactions were simulated according to the distribution given in Eq. (1.1), with a lower electron energy cutoff  $T_e^{\text{min}} = 0.1$  GeV. This cutoff ensures that the critical region between 0.1 and 2 GeV is fully simulated. In this region, the magnetic moment cross-section falls steeply while the experimental sensitivity increases slowly (see Fig. 1). The generated particles were then propagated through the detector in a GEANT Monte Carlo simulation [19]. The output was used to determine the selection efficiency for magnetic moment events. Similarly, the expected number of events from Standard Model processes was found from neutrino–nucleon interactions generated by LEPTO [20].

Two sets of well-understood and easily identifiable control events were used to study the magnetic moment cuts systematically, with a data sample and a Monte Carlo sample in each set. Comparing the fraction of events removed from the two samples by each selection cut provided an estimate of the systematic uncertainty and the difference between data and Monte Carlo. The first set consisted of  $\nu_\mu$  charged-current interactions containing a reconstructed muon, thus providing background events for this analysis. The second set consisted of events with an electromagnetic shower, thus providing signal events for this analysis. In this set, the data sample contained “knock-on” electrons that were produced when a high-momentum muon scattered off an electron in the target region. These electromagnetic showers were extracted from data runs with straight-through muons collected for calibration and alignment. The electron energy spectrum in these events drops as  $T^{-2}$  [21], which makes them well-suited to study the sensitivity of the signal to our set of cuts (see Eq. (1.1)).

Two different approaches were used to compare data to Monte Carlo for the two sets of control events. In one approach, the fraction of events removed by each cut from the full sample was found for data and Monte Carlo. Since each cut was applied to the entire sample of events, this gave an accurate estimate of the systematic uncertainty for each cut. No difference between data and Monte Carlo was found, with each cut removing the same fraction of events from both data and Monte Carlo for both control sets within statistical uncertainty.

Dependencies between cuts were addressed in the second approach, in which all of the cuts were applied to a given sample. Each cut was applied only to the events that passed the previous cut. After each cut, the fraction of remaining events was compared between data and Monte Carlo. In this approach, the statistical uncertainty increased with each cut as the number of remaining events decreased. Again, no difference was found between data and Monte Carlo for both control sets within statistical uncertainty.

## 5. Results and discussion

The single event surviving all cuts is shown in Fig. 4. This neutrino interaction occurred in the most downstream emulsion module and produced a narrow shower of particles with a reconstructed track at its center that had an angle of  $(10 \pm 5)$  mrad with respect to the neutrino direction. The total recorded signal in the calorimeter was 20.0 GeV, of which 16.8 GeV were associated with the central part of the electromagnetic shower. For this energy, the electron angle should be less than 7 mrad according to Eq. (1.2). The selected event could be a quasi-elastic  $\nu_e$ -N interaction with a relatively low-energy neutrino.

A selection efficiency for magnetic moment events of  $(9.0 \pm 0.6)\%$  was found in the Monte Carlo study. The expected background rate due to neutrino–nucleon scattering was 2.3 events and other processes, such as weak neutrino–electron scattering, are expected to contribute less than 0.05 events. As we observed one event when the expected background rate was 2.3 events, we did not observe any signal events and the measured magnetic moment is zero. A statistical analysis based on the Feldman–Cousins method [22] yields a 90% upper confidence limit of 2.3 events in the signal.

To convert this limit on the number of signal events to a limit on the tau-neutrino magnetic moment, Eq. (1.1) is integrated numerically, taking into account the  $\nu_\tau$  energy spectrum. The resulting cross-section is

$$\sigma_{\text{tot}}^\mu = \frac{\mu_\nu^2}{\mu_B^2} \times 1.8 \times 10^{-28} \text{ m}^2. \quad (5.1)$$

A total of  $3.56 \times 10^{17}$  protons on target were used in generating this sample. The average target mass

during the run was 554 kg, corresponding to  $1.7 \times 10^{29}$  target electrons. The number of expected events for a magnetic moment  $\mu_\nu$  is then given by the product of flux, cross-section, and number of scattering centers, or:

$$n_{\text{events}} = \frac{\mu_\nu^2}{\mu_B^2} \times 1.5 \times 10^{13}. \quad (5.2)$$

This gives a limit for the magnetic moment of  $\mu_\nu < 3.9 \times 10^{-7} \mu_B$ . For comparison, the experimental sensitivity is  $4.9 \times 10^{-7} \mu_B$ , which is the limit that would be obtained had we observed as many events as predicted for the background.

This analysis is flavor-blind and the limit applies in principle to the sum over all neutrino flavors. However, more stringent limits have been determined by other experiments for  $\nu_e$  and  $\nu_\mu$ . Assuming a magnetic moment at the current limit, their contribution would be less than  $10^{-4}$  events. The limit is therefore interpreted as a new upper limit on  $\nu_\tau$ .

While systematic uncertainties were not included in this analysis as they are not part of the Feldman–Cousins method, they would only change the result slightly because the uncertainty due to Poisson statistics completely dominates the estimate of the limit. Contributions to the systematic uncertainty come from the neutrino flux calculation (15%), the total proton flux (15%), and the number of generated Monte Carlo events (5%). In addition to the statistical analysis based on the Feldman–Cousins method, a Bayesian analysis was performed [23] including all these systematic uncertainties using a flat prior distribution in the magnetic moment. This yields a 90% confidence limit of  $\mu_{\nu_\tau} < 3.5 \times 10^{-7} \mu_B$ . We include this result for comparison, only the upper limit derived with the Feldman–Cousins method should be quoted.

## 6. Conclusions

The new upper limit for the tau-neutrino magnetic moment of  $3.9 \times 10^{-7} \mu_B$  is an improvement over the previous limit [5]. Moreover, this is the first experiment to directly observe that the  $\nu_\tau$  component in the neutrino beam is at the expected level.

The new limit is still three orders of magnitude above the limits for  $\nu_e$  and  $\nu_\mu$ , and it dominates when extracting limits for the mass eigenstates from the

current limits for the flavor eigenstates. Improving the limit on  $\mu_{\nu_\tau}$  would require a  $\nu_\tau$  beam that is comparable in total flux to previous  $\nu_e$  and  $\nu_\mu$  beams.

## Acknowledgements

We gratefully acknowledge the ingenuity and support given to us by the staffs at Fermilab and at the collaboration universities. This work is supported by the General Secretariat of Research and Technology of Greece, the Japan Society for the Promotion of Science, the Japan–US Cooperative Research Program for High Energy Physics, the Ministry of Education, Science and Culture of Japan, the Korea Research Foundation Grant, and the United States Department of Energy.

## References

- [1] A.V. Derbin, *Phys. Atom. Nucl.* 57 (1994) 222.
- [2] LAMPF experiment 225, D.A. Krakauer et al., *Phys. Lett. B* 252 (1990) 177.
- [3] V.N. Trofimov, B.S. Neganov, A.A. Yukhimchuk, *Phys. Atom. Nucl.* 61 (1998) 1271.
- [4] A.G. Beda, E.V. Demidova, A.S. Starostin, M.B. Voloshin, *Phys. Atom. Nucl.* 61 (1998) 66.
- [5] WA66 Collaboration, A.M. Cooper-Sarkar, S. Sarkar, J. Guy, W. Venus, P.O. Hulth, K. Hultqvist, *Phys. Lett. B* 280 (1992) 153.
- [6] M. Talebazadeh et al., *Nucl. Phys. B* 273 (1987) 503.
- [7] DELPHI Collaboration, P. Abreu et al., *Z. Phys. C* 74 (1997) 577.
- [8] L3 Collaboration, M. Acciarri et al., *Phys. Lett. B* 412 (1997) 201.
- [9] N. Tanimoto, I. Nakano, M. Sakuda, *Phys. Lett. B* 478 (2000) 1.
- [10] SuperKamiokande Collaboration, Y. Fukuda et al., *Phys. Rev. Lett.* 81 (1998) 1562.
- [11] Soudan 2 Collaboration, W.W.M. Allison et al., *Phys. Lett. B* 449 (1999) 137.
- [12] S.M. Bilenky, C. Giunti, W. Grimus, *Eur. Phys. J. C* 1 (1998) 247.
- [13] J.F. Beacom, P. Vogel, *Phys. Rev. Lett.* 83 (1999) 5222.
- [14] S.N. Gninenko, N.V. Krasnikov, *Phys. Lett. B* 490 (2000) 9.
- [15] G. Domogatskii, D. Nadzhin, *Sov. J. Nucl. Phys.* 12 (1971) 678.
- [16] G. Rädcl, R. Beyer, *Mod. Phys. Lett. A* 8 (1993) 1067.
- [17] DONUT Collaboration, K. Kodama et al., *Phys. Lett. B* 504 (2001) 218.
- [18] R. Schwienhorst, Ph.D. Thesis, University of Minnesota, 2000.
- [19] R. Brun et al., GEANT Detector Description and Simulation Tool, CERN Program Library, 1994, W5013.
- [20] G. Ingelman, J. Rathsman, A. Edin, LEPTO — The Lund Monte Carlo for deep inelastic lepton–nucleon scattering, *Comput. Phys. Commun.* 101 (1997) 108.
- [21] A. Van Ginneken, *Nucl. Instrum. Methods A* 251 (1986) 21.
- [22] G.J. Feldman, R.D. Cousins, *Phys. Rev. D* 57 (1998) 3873.
- [23] G. D’Agostini, CERN Yellow report CERN-99-03, 1999.